Parity assignment for low-lying dipole states in ^{58}Ni

T. Shizuma [●],[1] M. Omer [●],[2,*] T. Hayakawa [●],[1,3] F. Minato [●],[4] S. Matsuba,[5] S. Miyamoto [●],[6]
N. Shimizu [●],[7] and Y. Utsuno [●][8,9]

[1]*Foundational Quantum Technology Research Directorate, National Institutes for Quantum Science and Technology, Kizugawa, Kyoto 619-0215, Japan*

[2]*Integrated Support Center for Nuclear Nonproliferation and Nuclear Security, Japan Atomic Energy Agency, Tokai, Ibaraki 319-1195, Japan*

[3]*Institute of Laser Engineering, Osaka University, Suita, Osaka 565-0871, Japan*

[4]*Department of Physics, Kyushu University, Nishi-ku, Fukuoka 819-0395, Japan*

[5]*Quantum Medical Science Directorate, National Institutes for Quantum Science and Technology, Inage, Chiba 263-8555, Japan*

[6]*Laboratory of Advanced Science and Technology for Industry, University of Hyogo, Kamigori, Hyogo 678-1205, Japan*

[7]*Center for Computational Sciences, University of Tsukuba, Tsukuba, Ibaraki 305-8577, Japan*

[8]*Advanced Science Research Center, Japan Atomic Energy Agency, Tokai, Ibaraki 319-1195, Japan*

[9]*Center for Nuclear Study, The University of Tokyo, Bunkyo-ku, Tokyo 113-0033, Japan*

Low-lying dipole states in the singly closed-shell nucleus ^{58}Ni were studied via nuclear resonance fluorescence experiments using a quasimonoenergetic, linearly polarized photon beam. The parity quantum numbers of the dipole states were determined by the intensity asymmetry of resonantly scattered γ rays with respect to the polarization plane of the incident photon beam. The electric and magnetic dipole ($E1$ and $M1$) strengths at excitation energies between 5.9 and 9.8 MeV were obtained based on dipole strengths taken from literature. The $E1$ and $M1$ strength distributions were compared with large-scale shell-model predictions in the fp shell using the SDPFSDG-MU interaction.

I. INTRODUCTION

Low-energy electric and magnetic dipole ($E1$ and $M1$) excitations have been the subject of considerable interest in nuclear structure physics [1–3]. The observation of $E1$ and $M1$ resonances provides information on collective and single-particle motions such as the $E1$ pygmy dipole resonance (PDR) as well as the spin-flip $M1$ resonance. In this paper, we discuss $E1$ strength of isovector type.

A concentration of $E1$ strengths has been observed in the vicinity of the particle thresholds in both stable and unstable nuclei, for example, in O [4], Ca [5], Ni [6,7], Kr [8], Sn [9–11], Xe [12,13], Ba [14], and Pb [15] isotopes. It is commonly referred to as PDR, because the strength is weak relative to that of the giant dipole resonance (GDR), which is the dominant part of the $E1$ strength in atomic nuclei. In a geometrical picture, the PDR is often associated with a vibration of the neutron skin against an almost $N \approx Z$ core [16]. The PDR strength is correlated with neutron skin thickness [17], which is related to the equation of state (EOS) of the neutron-rich matter [18]. The total sum of the measured energy-weighted PDR strength is less than 1% of the Thomas-Reiche-Kuhn (TRK) sum rule value for stable nuclei and less than 5% for unstable neutron-rich nuclei. For stable fp-shell nuclei, a smaller low-energy $E1$ strength, corresponding to

0.1–0.3% of the TRK sum rule value, is known [19–25]. In addition to $E1$ resonances, $M1$ strengths, mainly due to one-particle–one-hole (1p-1h) excitation of $(1f_{7/2}^{-1}, 1f_{5/2}^{1})$ for both protons and neutrons, have been observed in stable fp-shell nuclei [19–27].

The singly closed-fp-shell nucleus ^{58}Ni is suitable to study both $E1$ and $M1$ strengths. So far, the information on the dipole excitation has been obtained from measurements using nuclear resonance fluorescence (NRF) [19,21,28,29], in which the angular momentum $L = 1$ is predominately transferred by incident photons and therefore resonant states with spins and parities of $J^{\pi} = 1^{+}$ or 1^{-} are excited from the ground state in an even-even nucleus [30,31]. In the previous NRF measurement with partially polarized bremsstrahlung, 42 $J = 1$ states in ^{58}Ni were observed in the energy region between 5 and 10 MeV and the parity quantum numbers were assigned to the 18 $J = 1$ states [19]. Furthermore, those for the additional 12 $J = 1$ states were obtained in an NRF measurement with a quasimonoenergetic, linearly polarized photon beam [21]. However, above 9.5 MeV, the information on parities are still missing.

In this paper, we present results of an NRF measurement on ^{58}Ni using a quasimonoenergetic, linearly polarized photon beam. The parities were determined by intensity asymmetry of resonant γ rays with respect to the polarization plane of the incident photon beam. The $M1$ and $E1$ strengths were obtained based on the previously known dipole strengths [19]. The results were compared with those obtained from

*Present address: Physics Department, Faculty of Science, Assiut University, Assiut 71516, Egypt.

large-scale shell-model calculations using the SDPFSDG-MU interaction.

II. EXPERIMENTAL PROCEDURE

The present NRF measurement was carried out at the NewSUBARU synchrotron radiation facility at the University of Hyogo [32,33]. A quasimonoenergetic, linearly polarized photon beam was generated by backward Compton scattering of laser photons with electrons circulating in the NewSUB-ARU storage ring. A Nd:YVO$_4$ laser with a wavelength of 1064 nm was used at a frequency of 20 kHz. The electron energies were selected as 578, 625, 670, 694, 714, 735, and 761 MeV to produce LCS photon beams with maximum energies E_γ^{max} of 6.1, 7.1, 8.2, 8.8, 9.3, 9.8, and 10.5 MeV, respectively. A lead collimator with a 10-cm thickness and 5-mm aperture was used to form a quasi-monoenergetic photon beam with an energy spread of $\Delta E/E = 3\%$ to 5% at full width at half maximum (FWHM). The photon flux was measured using a large volume (8 in. × 12 in.) NaI(Tl) scintillation detector. The average intensity was 6×10^5 photons per second.

The target consisted of a metallic cylinder (8 mm in diameter) of ^{58}Ni (10 g) enriched to 99.981%. Three high-purity germanium (HPGe) detectors with detection efficiencies of 70%, 120%, and 140% relative to a 3 in. × 3 in. NaI scintillation detector were used to measure scattered photons from the target at a scattering angle of $\theta = 90°$. While two of the detectors (70% and 140%) were placed in the vertical plane, the other (120%) was in the horizontal plane. The typical energy resolution of the HPGe detectors was $\Delta E_\gamma/E_\gamma \approx 0.09\%$ at $E_\gamma \approx 7$ MeV. The γ-ray energies were calibrated using a natural background line (2614 keV) as well as resonance lines (5511, 7063, 7083, 7178, 7209, 7246, 7280, 7299, and 7332 keV) of ^{208}Pb.

The intensity asymmetry of the resonantly scattered photons with respect to the polarization plane of the incident photon beam can be used for parity determination [34]. The azimuthal angular distribution of γ rays for dipole transitions is expressed as

$$W(\theta, \phi) = W(\theta) \mp \tfrac{3}{4}(1 - \cos^2\theta)\cos2\phi, \quad (1)$$

where θ is the scattering angle of photons with respect to the incoming photon beam, and ϕ is the azimuthal angle between the polarization plane (formed by the propagation direction and the electric field vector of the incident photon beam) and the reaction plane. $W(\theta) \, (= 3/4 + 3/4\cos^2\theta)$ is the angular correlation function for unpolarized dipole radiation. Here, the minus (plus) sign corresponds to $E1$ ($M1$) transitions. In the present case ($\theta = 90°$), Eq. (1) can be reduced to

$$W(90°, \phi) = \tfrac{3}{4}(1 \mp \cos2\phi). \quad (2)$$

A more general form of Eq. (1) can be found in Ref. [35].

The analyzing power is defined in Ref. [34] using the azimuthal angular distributions at $\phi = 0°$ and $90°$ as

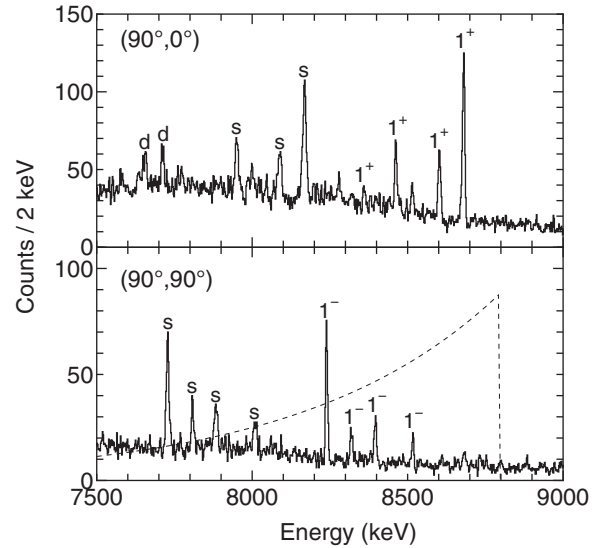$$\Sigma = \frac{W(90°, 0°) - W(90°, 90°)}{W(90°, 0°) + W(90°, 90°)}. \quad (3)$$

FIG. 1. A typical photon scattering spectrum observed at polar and azimuthal angles of $(\theta, \phi) = (90°, 0°)$ and $(90°, 90°)$ from the measurement with the maximum beam energy of $E_\gamma^{max} = 8.8$ MeV. The J^π assignments are indicated for the ground state transitions in ^{58}Ni. Peaks labeled s and d are due to single and double escapes, respectively. The dashed line shows the energy distribution of the incident photon beam.

Under the condition of complete polarization of the incoming photon beam, $\Sigma = +1$ is expected for $M1$ transitions, and $\Sigma = -1$ is expected for $E1$ transitions.

The corresponding intensity asymmetry of the observed NRF γ rays is given by

$$A = \frac{N_\parallel - N_\perp}{N_\parallel + N_\perp} = q\Sigma, \quad (4)$$

where $N_\parallel$ ($N_\perp$) represents the measured intensity of NRF γ rays detected at $\theta = 90°$ in the plane parallel (perpendicular) to the polarization plane. Here, q is the experimental sensitivity, which is less than unity because of the finite solid angle of each HPGe detector and the spatially extended target. In the present case, q is estimated to be 0.85 by a numerical simulation. Thus, based on the azimuthal intensity asymmetry, the multipolarities ($E1$ or $M1$) of resonantly scattered transitions can be determined.

III. RESULTS

Figure 1 shows a typical photon scattering spectrum obtained at the polar and azimuthal angles of $(\theta, \phi) = (90°, 0°)$ and $(90°, 90°)$ from the measurement with the maximum beam energy of $E_\gamma^{max} = 8.8$ MeV. Peaks shown with spin and parity represent ground state transitions. In the previous NRF measurement [19], 42 resonant states mostly with $J = 1$ were observed at excitation energies between 5 and 10 MeV. We confirmed a total of 31 states, including a state at 9843 keV reported by Ackermann *et al.* [29]. The lowest integrated cross section I_s observed in the present measurement is estimated to be as low as 10 eV b from comparison with the previous NRF measurement [19]. Some of transitions with $I_s \gtrsim 10$ eV b, observed at 7249, 7766, 8096, 8552, and 9455 keV, could

not be confirmed. This may indicate that these transitions have smaller cross sections. In addition, inelastically scattered transitions observed at 6424, 6430, 6685, 6892, 7595, 7616, and 8068 keV in the previous measurement [19] could not be confirmed.

The parity of the excited states is given on the basis of the azimuthal intensity asymmetry from Eqs. (3) and (4). Parities assigned by Scheck *et al.* [21] could be confirmed except for the levels at 7272 and 7877 keV to which the different parity was given in this work. In addition, parties assigned by Bauwens *et al.* [19] for levels at 7807, 9523, and 9723 keV could be confirmed and for four levels at 7585, 9554, 9631, and 9668 keV the parities were assigned for the first time. Furthermore, the levels at 8512 and 8514 keV are deduced as a $J^\pi = 1^+$ and 1^- doublet from the measured azimuthal intensity asymmetry.

The reduced transition probabilities were extracted from the ground state decay width Γ_0 taken from Ref. [19], using the following relations:

$$B(E1)\uparrow = 2.866 \frac{\Gamma_0}{E_\gamma^3} \times 10^{-3} \; e^2\text{fm}^2, \quad (5)$$

$$B(M1)\uparrow = 0.2598 \frac{\Gamma_0}{E_\gamma^3} \; \mu_N^2, \quad (6)$$

where Γ_0 is given in meV and E_γ in MeV. The experimental results are summarized in Table I.

Among the dipole excitations in the $E_x = 5.9$–9.8 MeV region, 14 states were assigned $J^\pi = 1^+$ and 18 states were assigned $J^\pi = 1^-$ based on the azimuthal intensity asymmetry. Thus, the total $M1$ strength at this energy region amounts to $\Sigma B(M1)\uparrow = 3.89(10)\mu_N^2$, while the total $E1$ strength is $\Sigma B(E1)\uparrow = 83.3(20) \times 10^{-3} \; e^2\text{fm}^2$. Note that the $B(M1)$ and $B(E1)$ values for the 8512- and 8514-keV levels were obtained by using the measured azimuthal intensity asymmetry. The present values are greater than the values of $\Sigma B(M1)\uparrow = 2.71(7)\mu_N^2$ and $\Sigma B(E1)\uparrow = 60.7(11) \times 10^{-3} \; e^2\text{fm}^2$ previously reported in Ref. [19].

IV. DISCUSSION

A. Large-scale shell-model calculations

In this section, the experimental $E1$ and $M1$ strength distributions in ^{58}Ni are compared with results of large-scale shell-model calculations. The present shell-model calculations were performed using the KSHELL code [37]. The model space of the present study is taken as $0\hbar\omega$ ($1\hbar\omega$) configurations in the sd, pf, and sdg shells for natural (unnatural) parity states. In addition, the excitation from the $0f_{7/2}$ orbit is restricted up to four-particle–four-hole excitations. As for the shell-model Hamiltonian, we adopt the SDPFSDG-MU interaction [38]. Its matrix elements in the sd and pf shells are the same as those of the SDPF-MU interaction [39], and the remaining ones are calculated with a variant of the monopole-based universal interaction [40] that was employed for the SDPF-MU interaction. The $E1$ strength distribution in ^{48}Ca was successfully reproduced with the $1\hbar\omega$ shell-model calculation that was used the SDFPSDG-MU interaction [41].

The $M1$ reduced transition strengths were calculated with effective g factors of $g_s^{\text{eff}} = 0.75 g_s^{\text{free}}$ for both protons and
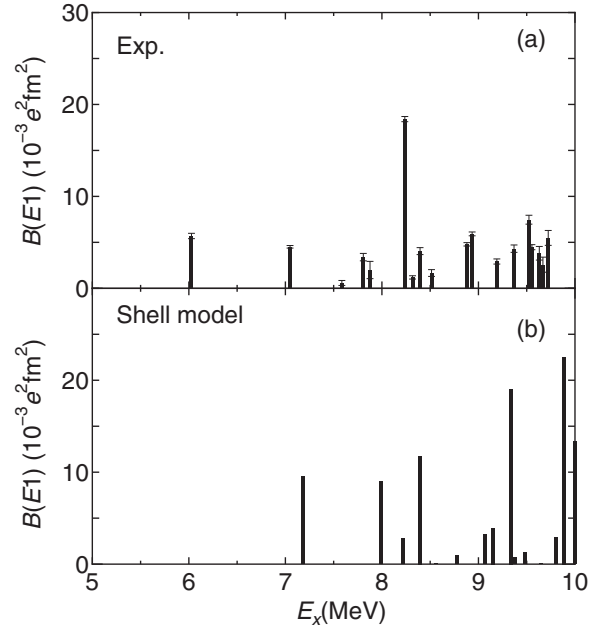

FIG. 2. Experimental $E1$ strength distribution below 10 MeV in ^{58}Ni compared with shell-model calculations with $B(E1)\uparrow > 0.2 \times 10^{-3} \; e^2\text{fm}^2$.

neutrons, which is a typical choice of shell-model studies of pf-shell nuclei (e.g., [42,43]). For $E1$ transitions, the effective charges are taken as $(e_p, e_n) = (N/A, -Z/A)e$, which are the bare charges subtracted by the contribution of the center-of-mass motion [44]. Note that the $E1$ and $M1$ strengths are described in a single framework.

B. $E1$ strength

The total $E1$ strength of ^{58}Ni at $E_x = 5.9$–9.8 MeV was determined to be $\Sigma B(E1)\uparrow = 83.3(20) \times 10^{-3} \; e^2\text{fm}^2$, corresponding to $\approx 0.33\%$ of the energy-weighted TRK sum rule value. Similar concentration of $E1$ strength was observed for the neighboring fp-shell nuclei [19–25]. The $E1$ strength concentration is discussed in relation to the so-called pygmy resonance for ^{54}Cr [45] and ^{60}Ni [7]. The strongest $E1$ transition was found at the excitation energy of 8237 keV with $B(E1)\uparrow = 18.41(28) \times 10^{-3} \; e^2\text{fm}^2$. Such strong $E1$ transitions have been observed in the neighboring nuclei with $N \approx Z \approx 28$, for example in ^{54}Fe [25] and ^{56}Fe [19] where the strongest $E1$ transitions in the same energy region were observed at 8015 and 8240 keV, respectively, with $B(E1)\uparrow = 10.7(1)$ and $18.51(2) \times 10^{-3} \; e^2\text{fm}^2$.

The experimental $E1$ strength distribution at excitation energies below 10 MeV is compared with the results of the shell-model calculations in Fig. 2. A total of 15 $J^\pi = 1^-$ states with ground-state excitation strengths greater than $B(E1)\uparrow = 0.2 \times 10^{-3} \; e^2\text{fm}^2$ are obtained in the calculation. The calculated $E1$ strength and the energy-weighted $E1$ strength below 9.8 MeV are $\Sigma B(E1)\uparrow = 87.7 \times 10^{-3} \; e^2\text{fm}^2$ and $\Sigma E_x B(E1)\uparrow = 784 \times 10^{-3} \; e^2\text{fm}^2$ MeV (0.37% of the TRK value), respectively, as summarized in Table II. Although the strength is less fragmented compared to the experimental one, the calculated total $E1$ strength is comparable with the

TABLE I. Parity assignments of the observed resonant states in ^{58}Ni obtained using the azimuthal intensity asymmetry A. Reduced transition probabilities $B(\sigma\lambda)\uparrow$ were calculated using information on ground state decay widths Γ_0 taken from Ref. [19].

E_x (keV)	E_x^a (keV)	Γ_0^a (meV)	J^π	A	J^π	$B(E1)\uparrow$ ($10^{-3}\,e^2$fm^2)	$B(M1)\uparrow$ (μ_N^2)
5905.8(9)	5905.3(7)	18(3)	1^{+b}	0.77(8)	1^+		0.023(4)
6028.0(4)	6027.3(7)	435(22)^c	1^{-b}	−0.89(6)	1^-	5.69(29)	
7047.3(5)	7048.2(9)	552(17)	1^{-b}	−0.88(5)	1^-	4.52(14)	
7270.0(11)	7271.7(7)	456(45)	1^{+b}	0.83(7)	1^+		0.308(30)
7388.0(5)	7388.8(4)	457(24)	1^{+b}	0.83(6)	1^+		0.294(15)
7583.0(15)	7585.1(6)	89(41)		−0.84(7)	$(1)^{-d}$	0.584(269)	
7710.4(6)	7709.7(6)	632(23)	1^{+b}	0.87(6)	1^+		0.358(13)
7807.6(6)	7807.3(5)	564(67)	1^{-a}	−0.86(6)	1^-	3.40(40)	
7875.2(9)	7876.7(26)	340(160)^c	1^{+b}	−0.75(8)	1^-	1.99(94)	
8237.5(5)	8237.3(4)	3590(55)	1^{-b}	−0.92(5)	1^-	18.41(28)	
8317.0(9)	8317.1(17)	239(36)	1^{-b}	−0.84(6)	1^-	1.19(18)	
8394.0(7)	8395.1(12)	836(78)	1^{-b}	−0.79(6)	1^-	4.05(38)	
8459.9(6)	8461.0(7)	893(48)	1^{+b}	0.86(7)	1^+		0.383(21)
8512.6(9)	8514.1(4)	686(51)	1^{-b}	−0.04(19)	1^{+e}		0.138(33)^e
8514.8(7)					1^{-e}	1.67(37)^e	
8600.2(6)	8600.5(7)	803(80)	1^{+b}	0.85(6)	1^+		0.328(33)
8777.9(5)	8679.3(8)	2052(103)	1^{+b}	0.78(5)	1^+		0.815(41)
8857.2(7)	8857.4(6)	751(147)	1^{+b}	0.84(7)	1^+		0.281(55)
8880.4(7)	8880.2(6)	1170(45)	1^{-b}	−0.85(6)	1^-	4.79(18)	
8934.9(7)	8934.6(5)	1474(52)	1^{-b}	−0.83(6)	1^-	5.92(21)	
8961.6(7)	8961.3(7)	378(39)	1^{+b}	0.92(7)	1^+		0.136(14)
9073.0(8)	9073.4(6)	888(60)	1^{+b}	0.82(7)	1^+		0.309(21)
9157.9(6)	9156.9(7)	594(79)	1^{+b}	0.91(6)	1^+		0.201(27)
9191.0(8)	9190.7(5)	791(75)	1^{-b}	−0.64(7)	1^-	2.92(28)	
9327.2(9)	9326.4(8)	975(63)	1^{+b}	0.80(9)	1^+		0.312(20)
9368.6(8)	9368.5(6)	1238(115)	1^{-b}	−0.85(6)	1^-	4.32(40)	
9523.4(9)	9523.3(13)	2250(146)	1^{-a}	−0.88(6)	1^-	7.47(48)	
9553.6(8)	9554.0(21)	1362(84)	1^a	−0.87(5)	1^-	4.48(28)	
9633.6(8)	9630.5(24)	1189(230)^c	1^a	−0.84(6)	1^-	3.82(74)	
9668.0(9)	9667.8(15)	812(260)^c	1^a	−0.52(9)	1^-	2.57(82)	
9724.6(9)	9723.0(9)	1760(260)^c	$1^{(-)a}$	−0.85(6)	1^-	5.49(81)	
9843.0(15)	9843(5)^f	880^f	2^{+f}	0.79(9)	2^+	59^g	

[a]Values taken from Ref. [19] unless otherwise stated.
[b]Values taken from Ref. [21].
[c]Uncertainties taken from Ref. [36], which were extracted by using uncertainties in Γ_0/Γ values and cross sections as in Ref. [19].
[d]Assuming $J = 1$ because a competitive $M2$ transition is generally weak.
[e]Deduced as a $J^\pi = 1^-$ and 1^+ doublet. The corresponding ground state decay widths $\Gamma_0(E1)$ and $\Gamma_0(M1)$ were obtained from the measured azimuthal intensity asymmetries A using $\Gamma_0(E1) = \Gamma_0(0.85 - A)/1.7$ and $\Gamma_0(M1) = \Gamma_0 - \Gamma_0(E1)$. The $B(E1)$ and $B(M1)$ values in columns 6 and 7 were calculated using Eqs. (5) and (6) by replacing Γ_0 with $\Gamma_0(E1)$ and $\Gamma_0(M1)$, respectively.
[f]Taken from Ref. [29].
[g]$B(E2)\uparrow = 6201\frac{\Gamma_0}{E_\gamma^5}\,e^4 fm^4$.

experimental value. The 8237-, 8317-, and 8395-keV transitions are observed to carry approximately 30% of the strength in the energy range from 6 to 10 MeV. The predicted $E1$ strengths at 7.99, 8.22, and 8.39 MeV amount to $B(E1)\uparrow = 23.5 \times 10^{-3}\,e^2$fm^2, and cover the experimental strength in this energy region.

C. $M1$ strength

Figure 3 compares the experimental $M1$ strength distribution at excitation energies below 10 MeV with the results of the shell-model calculations. A total of 51 $J^\pi = 1^+$ states are

obtained between 5.9 and 9.8 MeV in the present calculation. Out of these levels, only 39 states have ground-state excitation strength greater than $B(M1)\uparrow = 0.01\mu_N^2$, which corresponds roughly to the smallest experimental value. The strongest resonance is observed at the excitation energy of 8679 keV with $B(M1) = 0.815(41)\mu_N^2$, while the calculated maximum strength below 10 MeV is $B(M1)\uparrow = 0.51\mu_N^2$ at 9.6 MeV. Approximately 65% of the strength is accumulated in excitation energies between 8.4 and 9.4 MeV. In addition, a weaker $M1$ strength concentration is seen near 7.5 MeV. Similar strength concentrations are known for ^{50}Cr [27], ^{52}Cr [23,24], ^{54}Fe [25], ^{56}Fe [19,20,26], and ^{60}Ni [21]. The accumulation

TABLE II. Comparison of the experimental data with shell model calculations for the $E1$ strength in ^{58}Ni at excitation energies below 10 MeV. The total $E1$ strength $\Sigma B(E1)\uparrow$, energy weighted strength $\Sigma E_x B(E1)\uparrow$, and its value relative to the Thomas-Reiche-Kuhn (TRK) sum rule value are summarized.

	$\Sigma B(E1)\uparrow$ $(\times 10^{-3}\ e^2\text{fm}^2)$	$\Sigma E_x B(E1)\uparrow$ $(\times 10^{-3}\ e^2\text{fm}^2\ \text{MeV})$	$\Sigma E_x B(E1)\uparrow$ (%TRK)
Shell model	87.7	784	0.37
Experiment	83.3(20)	714(18)	0.33(8)

TABLE III. Comparison of the total $M1$ strengths $\Sigma B(M1)\uparrow$, the energy centroid E_c, and the variance σ_{E_c} in the energy range between 5.9 and 10 MeV.

	$\Sigma B(M1)\uparrow$ (μ_N^2)	E_c (MeV)	σ_{E_c} (MeV)
Shell model	3.8	8.9	0.99
Experiment	3.89(10)	8.5(3)	0.66(14)

of the $M1$ strengths near 8 and 9 MeV exhibits the typical pattern of the isoscalar and isovector $f_{7/2} \to f_{5/2}$ spin-flip $M1$ resonances [3,21]. The total $M1$ strength at excitation energies between 5.9 and 10 MeV is obtained to be $3.8\mu_N^2$ from the present shell-model calculation. This value is comparable with the measured value of $\Sigma B(M1)\uparrow = 3.89(10)\mu_N^2$. For a complete agreement, the fragmentation is somewhat overestimated.

To quantify the $M1$ strength distribution, the centroid energy E_c and its variance σ_{E_c}, defined by the following equations, were examined in the energy range between 5.9 and 10 MeV:

$$E_c = \Sigma\{E_x B(M1)\uparrow\}/\Sigma B(M1)\uparrow, \tag{7}$$

$$\sigma_{E_c} = [\Sigma\{(E_x - E_c)^2 B(M1)\uparrow\}/\Sigma B(M1)\uparrow]^{1/2}. \tag{8}$$

The results are shown in Table III. The calculated centroid is slightly larger than the experimental one. This suggests that missing smaller $M1$ strengths may exist and contribute to the fragmentation. It is also noted that the details of the
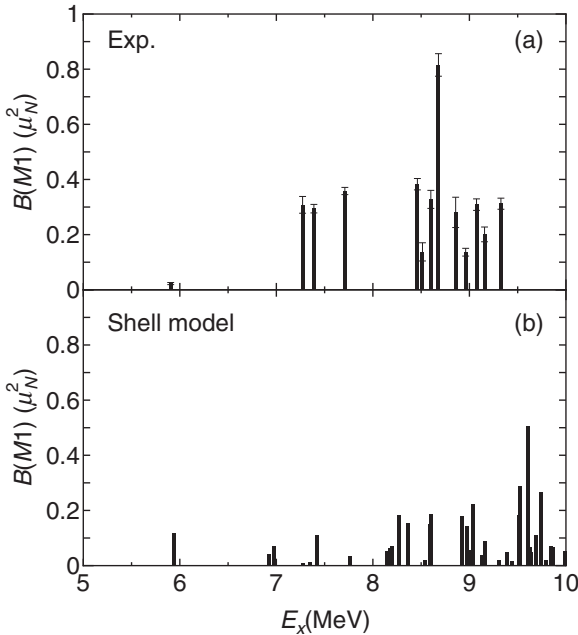
$M1$ strength distribution depend on the choice of the effective interaction as shown in the previous shell model calculations [20,46].

Figures 4(a) and 4(b) show spin (M_S) and orbital (M_L) components of the transition matrix elements (given by $B(M1) = [M_S + M_L]^2$) corresponding to the transitions presented in Fig. 3(b). As shown in Fig. 4, the strengths above $E_x \approx 7.5$ MeV are dominated by the spin component. Similar results are obtained in the previous shell-model calculations [20,26]. It should also be noted that the $M1$ strengths at excitation energies above ≈ 8.8 MeV are dominated by $f_{7/2} \to f_{5/2}$ spin-flip transitions, and that the proton and neutron contribute additively to the $M1$ operator with the proton contributing more than the neutron as shown in Fig. 5.

In a previous study, a microscopic quasiparticle phonon model (QPM) was used to calculate the 1^+ excited states in ^{58}Ni by including all one-phonon 1^+ configurations up to 15 MeV in the wave function [19]. The two-phonon configurations with excitation energies below 14 MeV and the three-phonon configurations were also included in the model space. The QPM calculations result in a double-humped structure formed by two strong excitations at 8.5 and 9 MeV [19]. The $M1$ strength contained at this energy region (8–10 MeV)
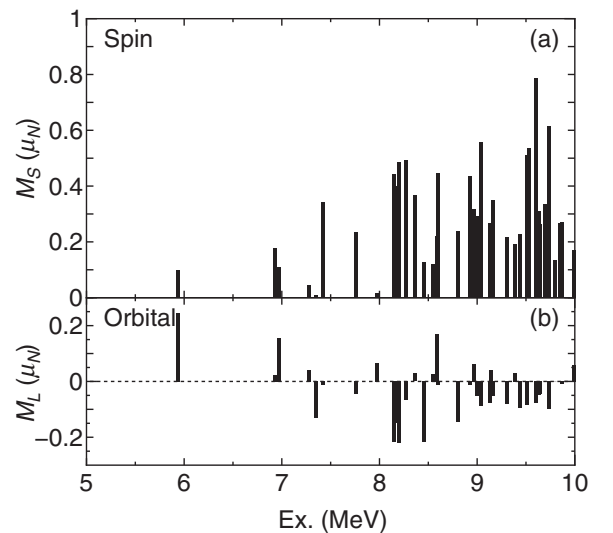

FIG. 3. Experimental $M1$ strength distribution below 10 MeV in ^{58}Ni compared with shell-model calculations with $B(M1)\uparrow > 0.01\mu_N^2$.

FIG. 4. Spin (M_S) and orbital (M_L) components of the transition matrix elements corresponding to the transitions shown in Fig. 3(b) obtained using the SDPFSDG-MU effective interaction. The $M1$ strength is given by $B(M1) = [M_S + M_L]^2$.
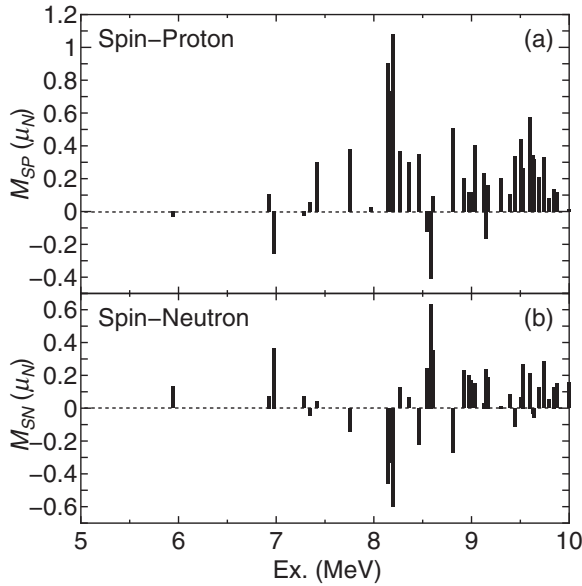
FIG. 5. Spin components of the transition matrix elements for (a) protons (M_{SP}) and (b) neutrons (M_{SN}) are shown. The total spin component shown in Fig. 4(a) is given by $M_S = M_{SP} + M_{SN}$.

was obtained to be $11\mu_N^2$, greater than the value obtained by the present shell-model calculations.

V. CONCLUSION

In conclusion, a photon scattering experiment on ^{58}Ni was carried out using a quasimonoenergetic, linearly polarized photon beam. A total of 31 states were confirmed at the energy region from 5.9 to 9.8 MeV. The parity quantum numbers were determined based on the intensity asymmetry of scattered γ rays with respect to the polarization plane of the incident photon beam. The total strengths of $\Sigma B(M1)\!\uparrow = 3.89(10)\mu_N^2$ and $\Sigma B(E1)\!\uparrow = 83.3(20) \times 10^{-3}$ e^2fm^2 at excitation energies between 5.9 and 9.8 MeV were obtained based on the dipole strengths previously reported. The observed $M1$ and $E1$ strengths of ^{58}Ni were compared with the results of the shell-model calculations in the fp shell using the SDPFSDG-MU interaction. The present shell-model calculation reproduced the gross properties of the total $E1$ and $M1$ strengths below ≈ 10 MeV.

[1] A. Bracco, E. Lanza, and A. Tamii, Prog. Part. Nucl. Phys. **106**, 360 (2019).

[2] D. Savran, T. Aumann, and A. Zilges, Prog. Part. Nucl. Phys. **70**, 210 (2013).

[3] K. Heyde, P. von Neumann-Cosel, and A. Richter, Rev. Mod. Phys. **82**, 2365 (2010).

[4] A. Leistenschneider, T. Aumann, K. Boretzky, D. Cortina, J. Cub, U. Datta Pramanik *et al.*, Phys. Rev. Lett. **86**, 5442 (2001).

[5] T. Hartmann, M. Babilon, S. Kamerdzhiev, E. Litvinova, D. Savran, S. Volz, and A. Zilges, Phys. Rev. Lett. **93**, 192501 (2004).

[6] O. Wieland, A. Bracco, F. Camera, G. Benzoni, N. Blasi, S. Brambilla *et al.*, Phys. Rev. Lett. **102**, 092502 (2009).

[7] M. Scheck, V. Yu. Ponomarev, T. Aumann, J. Beller, M. Fritzsche, J. Isaak *et al.*, Phys. Rev. C **87**, 051304(R) (2013).

[8] R. Schwengner, R. Massarczyk, G. Rusev, N. Tsoneva, D. Bemmerer, R. Beyer *et al.*, Phys. Rev. C **87**, 024306 (2013).

[9] K. Govaert, F. Bauwens, J. Bryssinck, D. De Frenne, E. Jacobs, W. Mondelaers, L. Govor, and V. Yu. Ponomarev, Phys. Rev. C **57**, 2229 (1998).

[10] P. Adrich, A. Klimkiewicz, M. Fallot, K. Boretzky, T. Aumann, D. Cortina-Gil *et al.*, Phys. Rev. Lett. **95**, 132501 (2005).

[11] A. Klimkiewicz, N. Paar, P. Adrich, M. Fallot, K. Boretzky, T. Aumann *et al.*, Phys. Rev. C **76**, 051603(R) (2007).

[12] D. Savran, M. Fritzsche, J. Hasper, K. Lindenberg, S. Müller, V. Yu. Ponomarev, K. Sonnabend, and A. Zilges, Phys. Rev. Lett. **100**, 232501 (2008).

[13] R. Massarczyk, R. Schwengner, F. Dönau, S. Frauendorf, M. Anders, D. Bemmerer *et al.*, Phys. Rev. Lett. **112**, 072501 (2014).

[14] A. P. Tonchev, S. L. Hammond, J. H. Kelley, E. Kwan, H. Lenske, G. Rusev, W. Tornow, and N. Tsoneva, Phys. Rev. Lett. **104**, 072501 (2010).

[15] N. Ryezayeva, T. Hartmann, Y. Kalmykov, H. Lenske, P. von Neumann-Cosel *et al.*, Phys. Rev. Lett. **89**, 272502 (2002).

[16] N. Paar, D. Vretenar, E. Khan, and G. Coló, Rep. Prog. Phys. **70**, R02 (2007).

[17] J. Piekarewicz, Phys. Rev. C **73**, 044325 (2006).

[18] B. A. Brown, Phys. Rev. Lett. **85**, 5296 (2000).

[19] F. Bauwens, J. Bryssinck, D. De Frenne, K. Govaert, L. Govor *et al.*, Phys. Rev. C **62**, 024302 (2000).

[20] T. Shizuma, T. Hayakawa, H. Ohgaki, H. Toyokawa, T. Komatsubara, N. Kikuzawa, T. Inakura, M. Honma, and H. Nakada, Phys. Rev. C **87**, 024301 (2013).

[21] M. Scheck, V. Yu. Ponomarev, M. Fritzsche, J. Joubert, T. Aumann, J. Beller *et al.*, Phys. Rev. C **88**, 044304 (2013).

[22] Krishichayan, M. Bhike, W. Tornow, G. Rusev, A. P. Tonchev, N. Tsoneva, and H. Lenske, Phys. Rev. C **91**, 044328 (2015).

[23] T. Shizuma, T. Hayakawa, I. Daito, H. Ohgaki, S. Miyamoto, and F. Minato, Phys. Rev. C **96**, 044316 (2017).

[24] J. Wilhelmy, B. A. Brown, P. Erbacher, U. Gayer, J. Isaak, Krishichayan *et al.*, Phys. Rev. C **98**, 034315 (2018).

[25] R. Schwengner, R. Massarczyk, R. Beyer, M. Bhike, B. A. Brown, Krishichayan *et al.*, Phys. Rev. C **101**, 064303 (2020).

[26] R. W. Fearick, G. Hartung, K. Langanke, G. Martínez-Pinedo, P. von Neumann-Cosel, and A. Richter, Nucl. Phys. A **727**, 41 (2003).

[27] H. Pai, T. Beck, J. Beller, R. Beyer, M. Bhike, V. Derya *et al.*, Phys. Rev. C **93**, 014318 (2016).

[28] F. R. Metzger, Nucl. Phys. A **158**, 88 (1970).

[29] K. Ackermann, K. Bangert, U. E. P. Berg, G. Junghans, R. K. M. Schneider, R. Stock, and K. Wienhard, Nucl. Phys. A **372**, 1 (1981).

[30] U. Kneissl, H. H. Pitz, and A. Zilges, Prog. Part. Nucl. Phys. **37**, 349 (1996).

[31] A. Zilges, D. L. Balabanski, J. Isaak, and N. Pietrall, Prog. Part. Nucl. Phys. **122**, 103903 (2022).

[32] S. Miyamoto, Y. Asano, S. Amano, D. Li, K. Imasaki, H. Kinugasa, Y. Shoji, T. Takagi, and T. Mochizuki, Radiat. Meas. **41**, S179 (2006).

[33] S. Amano, K. Horikawa, K. Ishihara, S. Miyamoto, T. Hayakawa, T. Shizuma, and T. Mochizuki, Nucl. Instrum. Methods Phys. Res., Sect. A **602**, 337 (2009).

[34] N. Pietralla, Z. Berant, V. N. Litvinenko, S. Hartman, F. F. Mikhailov *et al.*, Phys. Rev. Lett. **88**, 012502 (2001).

[35] L. W. Fagg and S. S. Hanna, Rev. Mod. Phys. **31**, 711 (1959).

[36] C. D. Nesaraja, S. D. Geraedts, and B. Singh, Nucl. Data Sheets **111**, 897 (2010).

[37] N. Shimizu, T. Mizusaki, Y. Utsuno, and Y. Tsunoda, Comput. Phys. Commun. **244**, 372 (2019).

[38] S. Yoshida, Y. Utsuno, N. Shimizu, and T. Otsuka, Phys. Rev. C **97**, 054321 (2018).

[39] Y. Utsuno, T. Otsuka, B. A. Brown, M. Honma, T. Mizusaki, and N. Shimizu, Phys. Rev. C **86**, 051301(R) (2012).

[40] T. Otsuka, T. Suzuki, M. Honma, Y. Utsuno, N. Tsunoda, K. Tsukiyama, and M. Hjorth-Jensen, Phys. Rev. Lett. **104**, 012501 (2010).

[41] Y. Utsuno, N. Shimizu, T. Otsuka, S. Ebata, and M. Honma, Prog. Nucl. Energy **82**, 102 (2015).

[42] P. von Neumann-Cosel, A. Poves, J. Retamesa, and A. Richiter, Phys. Lett. B **443**, 1 (1998).

[43] T. Suzuki and M. Honma, J. Phys.: Conf. Ser. **381**, 012118 (2012).

[44] P. Ring and P. Schuck, *The Nuclear Many-Body Problem* (Springer, New York, 2004).

[45] P. C. Ries, H. Pai, T. Beck, J. Beller, M. Bhike, V. Derya *et al.*, Phys. Rev. C **100**, 021301(R) (2019).

[46] A. L. Cole, T. S. Anderson, R. G. T. Zegers, S. M. Austin, B. A. Brown, L. Valdez, S. Gupta, G.W. Hitt, and O. Fawwaz, Phys. Rev. C **86**, 015809 (2012).